Design and Development of an X-Ray Streak Camera for Laser Produced Plasma Measurement

S. A. Letzring

Report No. 95
March, 1980

CHAPTER I

INTRODUCTION

The use of x-ray measurement techniques have proven to be important diagnostic tools in the analysis of the high temperature and high density conditions associated with laser produced plasmas. These diagnostic techniques include x-ray pinhole cameras and grazing incidence x-ray microscopes for the purpose of imaging the x-rays from the plasma, PIN photodiodes and scintillator-photomultiplier combinations viewing the plasma through absorbing foil filters for the purpose of electron temperature measurements, and x-ray line spectral measurements using grazing incidence crystal spectrographs and photographic film for the purpose of measuring the temperature, density and emission characteristics of various regions of the plasma.

Time resolved measurements are important in non-steady-state laser produced plasmas where characteristic time scales for x-ray emission are on the order of ten's of picoseconds. The development of time resolving instrumentation used in conjunction with the above x-ray diagnostic techniques is proving to be a valuable tool aiding in the understanding of laser produced plasma behavior.

An example of the type of measurement that can be carried out is the measurement of the collapse time of an imploding laser-

fusion pellet and a measurement of the hydrodynamic behvior of the pellet. This is accomplished by a spatially and temporally resolved measurement of the x-rays emitted by the laser heated target which allow one to measure directly the dynamics of the resulting implosion. Measurements of the trajectory in time and space of the x-ray emitting regions of the plasma allow one to deduce the actual trajectory of the imploding target and thereby compare measured implosion velocities and collapse times with calculated values.

An additional application is the measurement of time resolved x-ray spectra, i.e. continuum spectra or line spectra. This allows one to infer time dependent density and temperature behavior. Most recently, time resolved measurements of the x-ray signature of a laser produced plasma have been used as a diagnostic to measure transport properties of the plasma. This measurement is being carried out by measuring the collapse time of plastic coated spherical targets and then comparing this time with computer code predictions for various models of electron energy transport.

For typical laser produced plasma conditions, x-ray signatures are characterized by a small emitting region with spatial dimensions of tens of microns which emits x-rays in the energy range of several hundred electron volts to several kilo-electron volts on characteristic time scales of tens of picoseconds. The total x-ray energy emitted by the plasma can be several millijoules corresponding to fractions of a percent of the total laser energy absorbed by the target.

A more accurate estimate of the x-ray signature of a laser produced plasma can be made by calculating temperatures, scale lengths and times characteristic of conditions in a laser produced plasma.

A simple calculation, given below, of the maximum energy transferred from the laser radiation field to the electrons in the plasma shows that temperatures of 1-2 kev are typically expected.

Calculating the total radiation emitted per unit time by a unit volume of plasma containing N_i ions of charge Ze and N_e electrons with a velocity distribution f(v) gives

$$dJ_\nu = N_i N_e f(v')dv'dq_\nu(v')$$

The simplest approximation is to assume that the electrons have a Maxwellian velocity distribution

$$f(v) = \left(\frac{m}{2\pi kT_e}\right)^{3/2} 4\pi \exp\left(\frac{-mv^2}{2kT}\right)v^2$$

To find the total energy radiated dJ_ν must be integrated over all v. This expression is integrated from a v_{min} to infinity where v_{min} is given by:

$$\frac{1}{2} mv_{min}^2 = h\nu_{min}$$

Integrating over v one finds

$$J_\nu d_\nu = \left(\frac{32\pi}{3}\right)\left(\frac{2\pi}{3kT_e m}\right)^{1/2} \frac{Z^2 e^6}{mc^3} N_i N_e \exp(-h\nu/kT_e)d\nu$$

The "bound-free" interaction in which a free electron is captured into a bound state of an ion also results in the emission of a radiation continuum usually called recombination radiation. Stratton[1] points out that at high temperatures where one can assume that the ions are completely stripped, the recombination radiation will become negligible with respect to the Bremsstrahlung radiation for electron temperatures T_e and plasmas with atomic number Z such that

$$kT_e > 40Z^2 \quad \left(kT_e \text{ in ev} \right)$$

For low Z plasmas one can neglect recombination radiation but for a typical laser produced plasma with $kT_e = 1$ kev for $Z > 5$ one must start to include recombination radiation.

Recombination radiation has the same spectral dependence as Bremsstrahlung radiation with the exception that there are discontinuities at energies corresponding to the ionization energy at the series limit.

The last interaction mechanism in which an electron makes transitions between two bound states of an ion gives rise to discrete line spectra radiation. It is beyond the scope of this thesis to calculate either transition wavelengths or intensities; instead the more well-known results will be quoted.

The table below (from Stratton[1]) gives a compilation of several of the more important x-ray lines for low Z elements in the soft x-ray spectrum. Energies of the various lines are given in ev.

L_α and L_β are the usual Lyman α and Lyman β lines, LΔ is the Lyman series limit for the hydrogen-like ion, the $1s^2$ - $1s2p^2$ transition is the resonance line, and the $1s^2$ - $1s2p^3$ transition is the strong intercombination line.

TABLE I

Z	Element	L_α	L_β	L_Δ	$1s^2$ - $1s2p^1$	$1s^2$ - $1s2p^3$
6	C	368	435	490	309	305
7	N	500	593	667	430	426
8	O	652	775	873	574	569
9	F	800	984	1097	738	729
10	Ne	1025	1216	1361	922	915
11	Na	1240	1466	1647	1127	1117
12	Mg	1471	1744	1959	1352	1343
13	Al	1727	2046	2301	1598	1588
14	Si	2003	2375	2666	1865	1854

The previous discussion emphasized the requirements for the desired spectral range that a time resolving instrument should have. The discussion now turns to estimating the time scales of interest in a laser produced plasma.

The electron thermalization time is the shortest time scale of interest and can be estimated from Spitzer.[2]

$$t_{ee} = \frac{.266\, T^{3/2}}{N_e \ln \Lambda} \text{ sec} \qquad \left(\Lambda = \frac{3}{2} \left(\frac{K^3 T^3}{\pi N_e} \right)^{1/2} \left[\frac{1}{Ze^3} \right] \right) \qquad [T \text{ in } {}^\circ K]$$

For an 800 ev plasma ($T \simeq 10^6$ K), $N_e = 10^{21}$ cm^{-3} and, choosing 10 as an appropriate value for the Coulomb logarithm, ln Λ.

$$t_{ee} = .26 \times 10^{-13} \text{ sec}$$

The electron-ion thermalization time is the next larger time scale of interest and is longer by the ratio $m_{ion}/m_{electron}$. Therefore:

$$\tau_{ei} = \frac{252\ T_e^{3/2}\ A}{N_e\ Z^2\ \ln\ \Lambda} \quad \text{sec}$$

For typical low-Z plasmas obtained in laser pellet interactions this time is of the order of 10^{-11} to 10^{-12} seconds.

Two other time scales of interest are: (1) The time for an acoustic wave to propagate across the plasma and (2) the time scale appropriate for thermal conductivity. Writing the time for an acoustic wave to propagate through the plasma as

$$\tau_a = \frac{l}{c_s}$$

where l is some scale length of interest in the plasma and c_s is the speed of sound in the plasma. The sound velocity can be written as:

$$c_s = \sqrt{\frac{\gamma\ Zk\ T_e}{Am_{ion}}} \quad \text{cm sec}^{-1}$$

Assuming the plasma behaves as an ideal gas γ can be set equal to 5/3.

For a typical low-Z laser plasma at 1 kev electron temperature $c_s = 1\text{-}3 \times 10^7$ cm/sec. For scale lengths of interest of 10μ this leads to time scales on the order of 10^{-10} sec. Usually, however, local plasma dynamics is governed by the time scale for electron thermal conduction.

Consider the heat diffusion equation:

$$\frac{\partial T}{\partial t} = \chi \frac{\partial^2 T}{\partial x^2}$$

where $\chi = \dfrac{K_e}{C_v N_e}$

K_e = coefficient of electron thermal conductivity

C_v = heat capacity = 3/2 k for a perfect gas.

Spitzer[2] derives the electron thermal conductivity as:

$$K_e = \frac{2.7 \times 10^5 \, (kT_e)^{5/2}}{Z \ln \Lambda} \quad \frac{\text{ergs}}{\text{sec deg cm}} \quad (kT_e \text{ in ev})$$

Writing the time scale τ_H as

$$\tau_H = \frac{l_H^2}{\chi}$$

$$\tau_H = 7.7 \times 10^{-21} \; l_H^2 \; N_e Z (kT_e)^{-5/2}$$

For the following conditions: $N_e = 10^{21}$ cm^{-3}

$Z = 1$

$kT_e = 1$ kev

$l_H = 10\mu$

$$\tau_H = 2.4 \times 10^{-13} \text{ sec}$$

And for $l_H = 100\mu$, a typical target diameter, $\tau_H = 2.4 \times 10^{-11}$ sec.

It has been shown from looking at the fundamental time scales of physical processes occurring in the plasma that in order to resolve these basic processes the time resolution of the temporally resolving x-ray detector should be on the order of 10^{-12} to 10^{-13} seconds.

The spatial resolution required can be estimated by looking at the characteristic scale lengths associated with basic physical processes occurring in the plasma. To first approximation the scale length can be calculated by considering typical plasma expansion velocities and the distance a plasma can expand during a representative time scale. The plasma expansion velocity is just given by the thermal velocity

$$V_{th} = \sqrt{\frac{3kT_e}{M_i}} \quad \text{cm/sec}$$

where T_e as usual is the electron temperature and M_i is the ion mass. For an SiO_2 plasma at a temperature of 1 kev (this is typical of a glass microballoon plasma near the outer surface of the balloon) the expansion velocity is roughly 10^7 cm/sec or .1μ/picosecond. Therefore, for time scales of interest of ten's of picoseconds, this leads to spatial scales of interest of microns.

The objective of this thesis work was to develop an x-ray diagnostic with the capability of temporally and spatially resolving

the x-ray emission from a laser produced plasma. Ultimately, we wish to study the compression physics of inertially confined laser fusion targets.

As will be discussed in Chapter II of this thesis, groups in other laboratories were simultaneously developing similar diagnostics for similar purposes. No attempt was made to duplicate the work of these other groups. Rather, the design of the diagnostic was addressed from basic principles and an attempt was made to design a system with maximum flexibility.

The design criteria, design options and resultant engineering that went into the construction of the diagnostic will be discussed in Chapter III of this thesis. Chapter IV discusses the actual experimental measurements that were performed while Section V discusses the comparison between experimental measurements and theoretical predictions of the x-ray signature for certain classes of inertially confined laser fusion target implosions. Chapter VI will address the conclusions of this thesis work.

REFERENCES - CHAPTER 1

1. Stratton, T.F. "X-Ray Spectroscopy" in Plasma Diagnostic Techniques, Ed. by R. H. Huddlestone and S. L. Leonard, p. 359, Academic Press, New York (1965).

2. Spitzer, L. Jr. The Physics of Fully Ionized Gases, p. 133, Wiley, New York, (1960).

CHAPTER II

SURVEY OF TIME RESOLVED X-RAY TECHNIQUES

The preceeding arguments have made the case for developing time-resolved x-ray measurement capabilities. The specific type of device to develop remains to be defined. At the beginning of this thesis project in 1974 a survey was made of available techniques to time resolve x-ray emissions from laser produced plasmas. These techniques can be broadly divided into two major groups. First, spatially resolving techniques which utilize x-ray optics to spatially resolve the x-ray emissions and project the image onto a time-resolving image convertor which converts the x-ray image into either an electron or visible image; second, non-spatially resolving techniques utilizing spatially integrating devices which convert the x-ray photons to an electrical signal which is then displayed on an oscilloscope or other similar recording device.

The simplest, most direct technique used by many laboratories is to use a single x-ray detector (silicon PIN diode, photoelectric diode, pyroelectric detector) and a fast oscilloscope. However, these simple diagnostics are limited to a time resolution on the order of 100 picoseconds, due to the bandwidth limitations of the fastest available oscilloscopes. Commercially available oscilloscopes are limited to a bandwidth of 1 GHz (350 picoseconds

time resolution) in either the Tektronix 519 or the 7904/7A21. An experimental 5 GHz bandwidth (70 picoseconds time resolution) oscilloscope had been developed in France by Thomson CSF but was not in general use at that time. One such device is now available at the Laboratory for Laser Energetics (1979). The state of the art of fast x-ray detectors was well ahead of recording devices with at least one group reporting a photoelectric diode with a risetime of 30 picoseconds.[1] This is a very complex device, however, and more common devices have risetimes near 100 picoseconds.[2] Scintillator photomultiplier combinations are capable of similar time resolution. The fastest photomultiplier available is a 100 picosecond risetime crossed-field device,[3] but 300-500 picosecond risetime devices are available in more conventional designs.[4] Photomultipliers utilizing microchannel plates to provide the electron gain are also under consideration with risetimes of several hundred picoseconds.[5,6]

Many types of scintillators, plastic, liquid, and unitary crystal types were investigated and attempts were made to measure their rise and fall times. The shortest observed risetime for a plastic scintillator was 350 picosecond for Nuclear Enterprises type 111. This scintillator is made by mixing phenyl-biphenyl-oxidiazole into a matrix of polyvinyltoluene. Gallium activated ZnO has a decay time of 400 picoseconds and is expected to have a very short risetime although no measurements have been reported for it. Several liquid scintillators are reported to have risetimes of 100 picoseconds or less and one glass-like substance, TMQP,

has a risetime on the order of 50 picoseconds. Several unitary organic crystals such as anthracene and trans-stilbene are reported to have risetimes of 10 picoseconds or less but very long fall times so that the output has to be differentiated in order to recover the true time history of the x-ray flux.

In addition to oscilloscopes, several experimenters developed multi-channel, single-shot sampling systems for recording the output of x-ray detectors. Sampling heads with 20 picosecond risetime are commercially available although quite expensive.[7] This technique requires that the output of the diode, photomultiplier etc. be electrically divided into multiple outputs and then directed into an array of sampling heads each of which would then sample the waveform at a different time. This technique is shown schematically in Figure 1. This type of system was built by one research group using 10 sampling heads of 30 picoseconds risetime with an uncertainty of 160 picoseconds in the sampling time.[8] This system, when coupled with a photodiode of 30 picosecond response time, has an overall response time of 75 picoseconds. Optically triggered sampling systems show promise of having both better risetime and sampling time uncertainty and should greatly improve the overall response time of a sampling system.[9,10]

Another type of sampling system under development is a multi-channel time to amplitude converter. This system, shown schematically in Figure 2, consists of a wide-bandwidth signal divider and an array of fast precision discriminators set to trigger

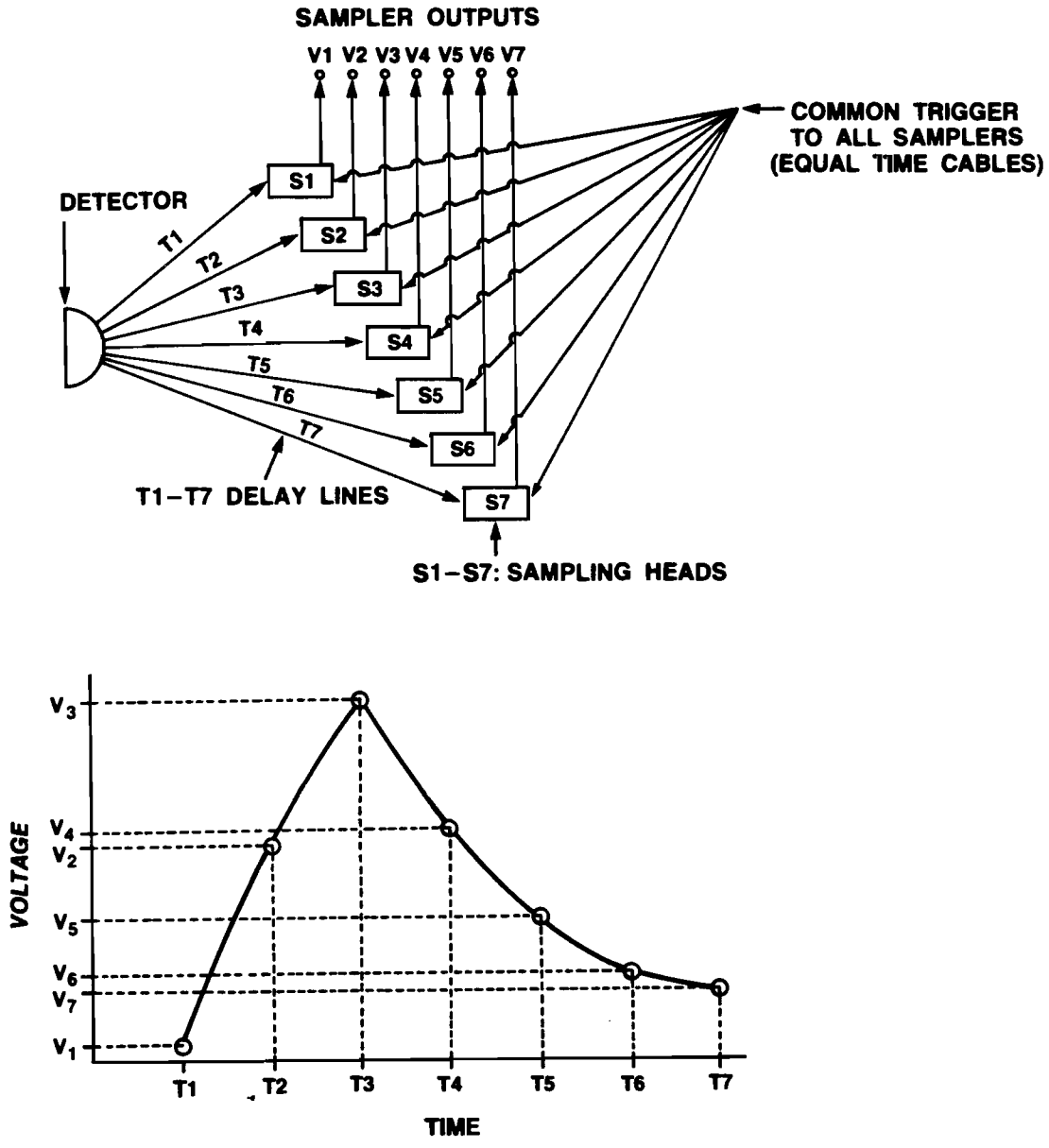

Figure 1. Multi-channel sampling system using synchronously triggered sampling gates.

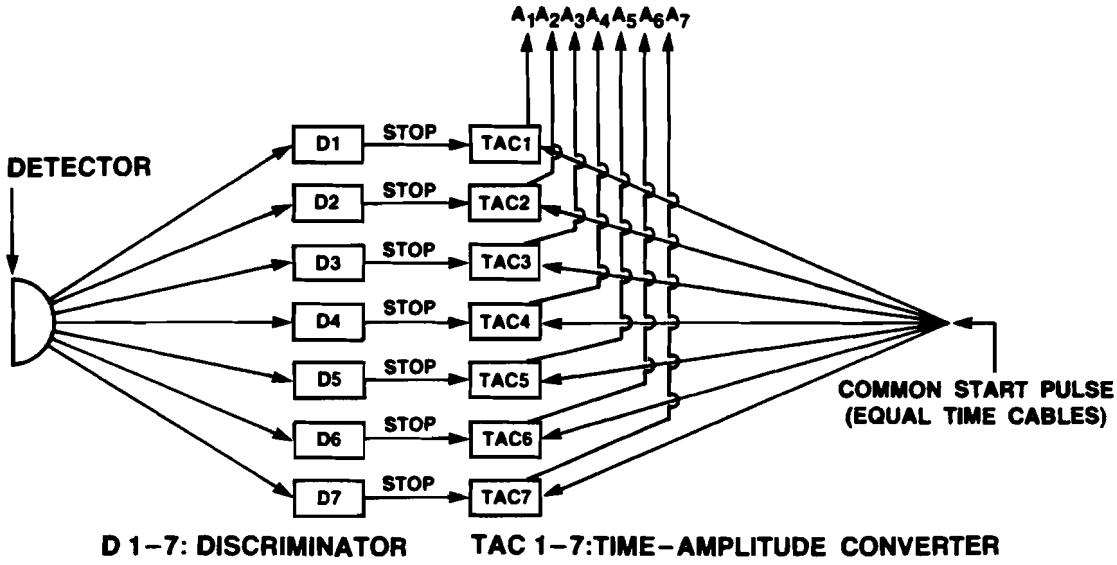

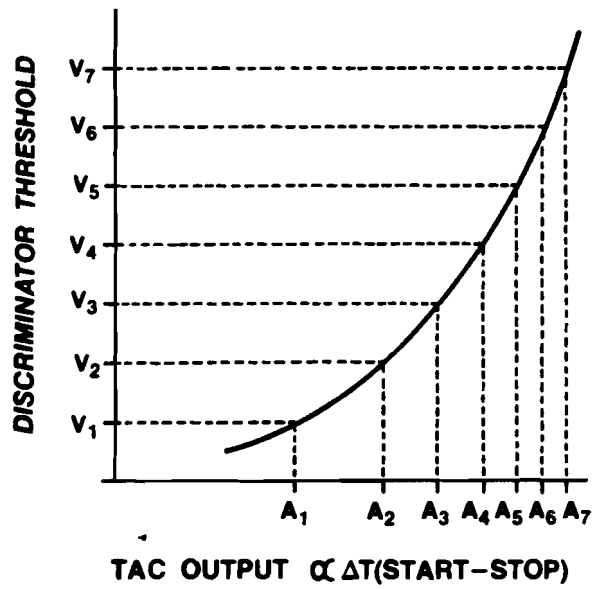

Figure 2. Multi-channel sampling system using discriminators and time-to amplitude converters.

at increasing voltage levels. The discriminator outputs then provide the stop pulses for an array of time-to-amplitude converters. The start pulse for each of the time-to-amplitude converters is a common initial trigger. The output of the array of time-to-amplitude converters is then a time history of the risetime of the input signal. The major drawback of this system is that it can only accept monotonically increasing voltage signals. An instrument is offered commercially which has a single channel resolution of 10 picoseconds and an overall system response of ±15 picoseconds.[11]

This general class of techniques consisting of a detector followed by a recording system has the sensitivity, dynamic range, and spectral range needed for a time-resolving diagnostic system. However, the marginal temporal resolution and the fact that the detectors are spatially integrating i.e. one detector would be needed per spatial resolution element, seems to limit the usefulness of this class of techniques as a primary x-ray diagnostic system.

The second class of detector systems, based on image conversion, seems to hold more promise. These systems are composed of an image converter section which changes the incoming time-dependent x-ray flux into a time-dependent electron beam, which is then passed through a time-analyzer, converted into visible photons and recorded on film or other suitable detector array. Two different types of systems were under consideration by various laboratories.

The first system was an optical streak camera system coupled to a fast scintillator. The x-rays are changed into visible photons by the scintillator which are then time-analyzed by the optical streak camera. There are many drawbacks to this type of system. The first and most important is the limited temporal resolution available with even the fastest scintillators. Other drawbacks are a tradeoff between sensitivity and spatial resolution in the scintillator. If the scintillator is thick enough to achieve high efficiency, spatial resolution will suffer because of the varying depths of emission of the visible photons from the scintillator.

Two such camera systems were built and tested. The first, at the Lebedev Institute,[12] uses a plastic scintillator containing the organic scintillator POPOP with a decay time of less than 500 picseconds. Very little was ever published about this camera and it doesn't seem to have been used past 1975. The other scintillator/streak camera system was constructed jointly by the United States Air Force Academy and the Battelle, Columbus Laboratories.[13] This camera used either anthracene or trans-stilbene as the scintillator and an IMACON streak camera. Quoted resolution is 10 picoseconds but very little data was ever published from this camera. Data reduction is very difficult in that the scintillator integrates the x-ray output because of its fast rise-time and slow fall-time so that the streak data has to be amplitude differentiated in order to recover the temporal history.

The other type of system under study in 1974 was the true x-ray streak camera in which an x-ray sensitive photocathode is used in a conventional streak tube to time resolve the x-ray flux from a laser produced plasma. Three laboratories were developing these x-ray streak cameras in 1974. A group at the Lebedev Institute[12] developed a very unique camera in that it has both a metallic x-ray photocathode and a Cs_3Sb visible photocathode deposited on a 5 micron thick mica substrate which is transparent to both visible and x-ray radiation. A second thin mica window served as the entrance window and vacuum seal for the tube. The calculated temporal resolution for this tube is 20 picoseconds based on a 60 kv/cm extraction field at the photocathode. This tube is based on the Russian PIM-UMI image converter tube with attached three-stage magnetically focused image intensifier.

A British group composed of experimentalists from Imperial College and The Queen's University of Belfast also developed an x-ray streak camera in 1974.[14] They use an open tube design based on an ITL Photocron I visible streak tube with the visible photocathode replaced with an x-ray sensitive one. This tube shares a common vacuum with the experimental chamber so it does not have to have an x-ray transparent, vacuum tight entrance window. Their first camera uses a reflective mode photocathode for higher quantum efficiency and it provides simultaneous spatial and temporal resolutions of 30 microns and 40 picoseconds, respectively.

The other camera under development in 1974 was a device at the Lawrence Livermore Laboratories.[15] This is a sealed design based on an RCA streak tube with a thin Be entrance window. This camera uses a metallic photocathode deposited on the inside of the Be entrance window. In its original tests, it exhibited a temporal resolution of 50 picoseconds.

Soon thereafter, x-ray streak cameras were developed at several other laboratories including Los Alamos,[16] NRC Canada,[17] and the Laboratory for Laser Energetics at the University of Rochester. The Los Alamos design is a totally new development effort based on an electron velocity preselector immediately after the photocathode and proximity focusing in the rest of the tube. The LLE design will be discussed in detail in Section III of this thesis.

Two design criteria which led to the final design of the LLE camera and which make it different from the other designs are: (1) the desire to have the widest possible spectral sensitivity and (2) the desire to have the most flexible arrangement possible for changing the photocathode and front end electron optics. Criteria (1) dictated a windowless design which would have to share a common vacuum with the experimental tank, while criteria (2) dictated a modular approach to the photocathode and extraction mesh assembly so that these could be changed quickly and easily. The adoption of these two basic design criteria along with the other features to be discussed in the next section have resulted in a unique new diagnositc tool.

REFERENCES - CHAPTER 2

1. M. Deloron, Acta Electronica, 15, 4, 265 (1972).
2. Developed at Laboratoires D'electronique et de Physique Appliquee, France.
3. Varian Type VPM 148.
4. J. Boutot, Acta Electronica, 15, 4, 271 (1972).
5. P. B. Lyons and J. Stevens, Nuclear Instruments and Methods, 114, 313, (1974).
6. F. T. Kuchnir, F. J. Lynch, I.E.E.E. Trans. Nucl. Sci., NS-15, 107 (1968).
7. Hewlett-Packard Model 1430C.
8. Lockheed Palo Alto Research Laboratory, Report C, April 1974.
9. J. R. Andrews and R. A. Lawton, Rev. Sci. Inst., Vol. 47, No. 3, 312, (1976).
10. G. Mourou, private communication.
11. Nanofast, Inc., Model 7004C-10P.
12. Bryukhnevitch, et. al., Proceedings of the 11th Congress on High Speed Photography. Chapman and Hall, London (1974), pp. 554-560.
13. R. A. Nuttelman, H. M. Epstein, J. W. Beal and P. J. Mallozzi, Advances in X-ray Analysis, Vol. 18, Plenum Press, (1974) pp. 197-203.

14. P. R. Bird, D. J. Bradley, A. G. Roddie, W. Sibbett, M. H. Key, M. J. Lamb and C. L. S. Lewis, Proceedings of the 11th Congress on High Speed Photography, Chapman and Hall, London (1974) pp. 118-123.

15. C. F. McConaghy and L. W. Coleman, Proceedings of the 11th Congress on High Speed Photography, Chapman and Hall, London (1974), pp. 196-201.

16. A. J. Lieber, et. al., Nucl. Inst. and Methods, 127, 87 (1975).

17. M. C. Richardson, private communication.

CHAPTER III

EXPERIMENTAL APPARATUS

The experimental objective of this thesis research was to develop an instrument to measure the temporally and spatially resolved x-ray emission from a laser produced plasma and then to compare the experimentally derived x-ray signatures with those predicted by computer code calculations.

To accomplish this objective an x-ray recording instrument which could simultaneously record temporally and spatially resolved x-ray emissions from a plasma of temperature around 1 kev, spatial dimensions of tens of microns and characteristic lifetimes of tens of picoseconds was designed and built. Comparable devices already exist for visible light sources - the visible streak camera. Figure 3 illustrates the main features of how an x-ray streak camera works.

The photon flux to be time resolved is imaged through a narrow input slit onto a photocathode. The electrons which are emitted by the photocathode are accelerated through the high electric field which exists between the photocathode and extraction mesh. The electron lens formed by the focusing cone and the anode structure images the photocathode onto a phosphor screen at the other end of the image converter tube. If the electron image of the slit were moved at a constant velocity across the phosphor screen in a

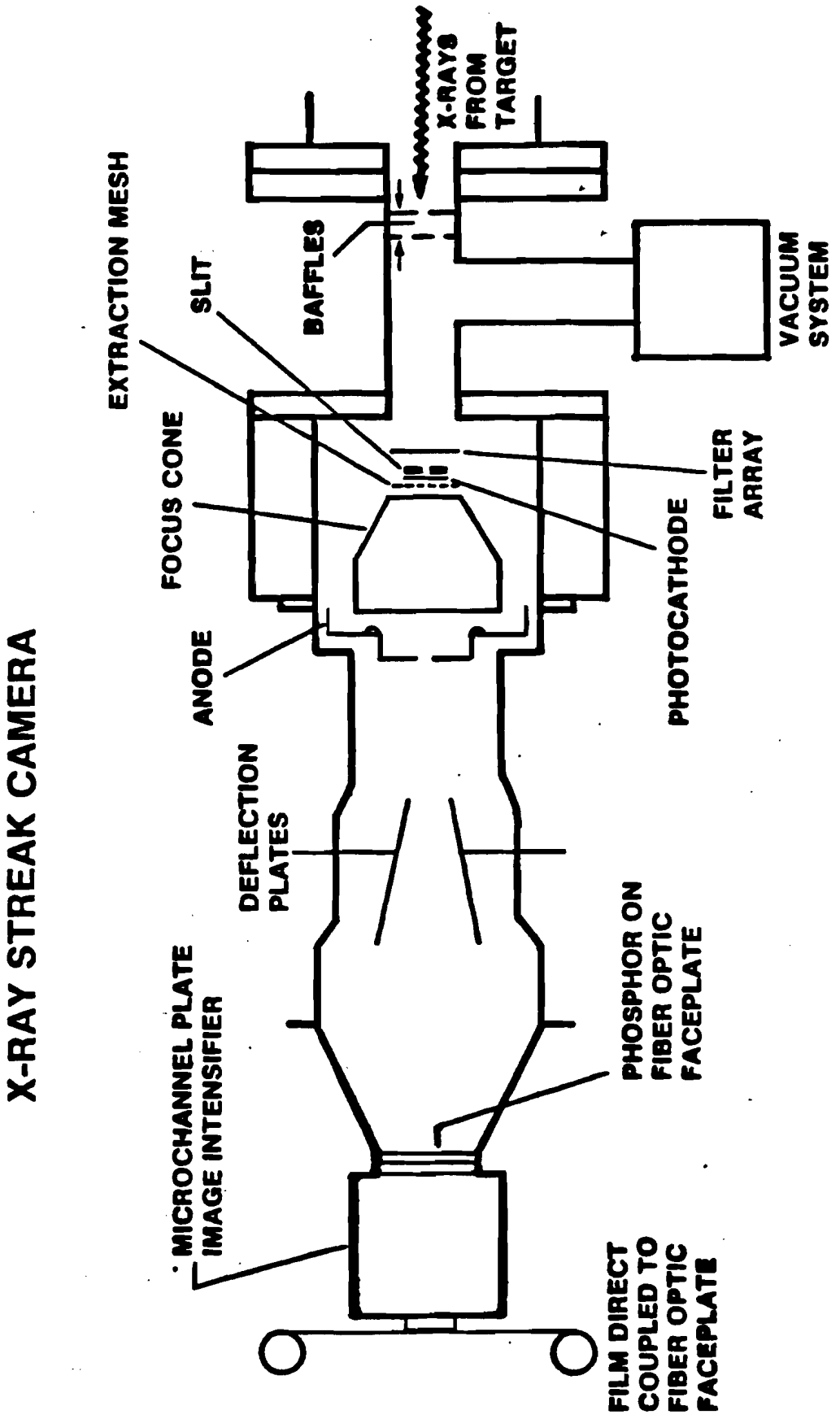
X-RAY STREAK CAMERA
X-RAYS FROM TARGET
EXTRACTION MESH
SLIT
BAFFLES
VACUUM SYSTEM
FOCUS CONE
FILTER ARRAY
PHOTOCATHODE
ANODE
DEFLECTION PLATES
MICROCHANNEL PLATE IMAGE INTENSIFIER
PHOSPHOR ON FIBER OPTIC FACEPLATE
FILM DIRECT COUPLED TO FIBER OPTIC FACEPLATE

Figure 3.

direction perpendicular to the long axis of the slit, the resultant image on the phosphor screen would be a "smeared" or "streaked" time history of the photon flux incident on the photocathode through the slit.

A. DESIGN GOALS

A set of design goals were decided upon for the construction of the x-ray streak camera. These were: (1) A temporal resolution of 15 picoseconds; (2) A spatial resolution of the x-ray camera of 5 line pair/mm which would result in a spatial resolution at the target of 10 microns when coupled with appropriate x-ray optics; (3) A sensitivity as close as possible to the theoretical minimum sensitivity of one photoelectron per resolution element; (4) Maximum dynamic range; (5) Spectral response from the near ultraviolet (5 ev or less) to tens of kev.

While all of these goals were not met exactly, experiments and calculations show that they were realistic expectations. Both calculations and measurement show that 20 picoseconds is probably the best temporal resolution available from the camera in its present form. Measurements show that the static spatial resolution of the system referred to the photocathode is somewhat better than the design goal, possibly as good as 8 line pair/mm. However, because of the poor spatial resolution of the x-ray optical system used to image the plasma, the best spatial resolution at the target is probably only 20 microns. The sensitivity of the camera is between

six and twelve photoelectrons per spatial and temporal resolution element, six being the lowest number of detectable photoelectrons capable of giving a statistically significant image. Dynamic range could not be measured. The spectral response is a function only of the photocathode and filters used and evidence will be shown that the expected response was indeed achieved.

These five design goals can be discussed in the context of the three most important characteristics of the camera system: temporal resolution, spatial resolution, and amplitude resolution. The last characteristic includes both sensitivity and dynamic range. The spectral range of the camera is not a characteristic of the camera system itself, but is determined by the choice of photocathode material and filters. This will be discussed in the photocathode section.

B. CHARACTERISTICS

Unfortunately, these three basic characteristics which describe the performance of the x-ray streak camera are not separable quantities and depend upon each other in a not well understood manner.

1. Temporal Resolution

Fortunately, at least one of the characteristics, the ultimate temporal resolution of the camera is calculable. This analysis follows one by Zavoisky and Fanchenko,[1] but is specialized to the case of an x-ray streak camera - their analysis being for an optical

streak camera. Many authors quote the time resolution of an x-ray streak camera as just the electron transist time dispersion first calculated by Korobkin, Maljutin and Schelev[2] as

$$\Delta\tau = 2.34 \times 10^{-8} \frac{(\Delta\varepsilon)^{\frac{1}{2}}}{E} \quad \text{sec}$$

where $\Delta\varepsilon$ = energy spread of photoelectrons in ev

E = electric field at photocathode in v/cm

This is a good approximation for an optical streak camera but a poor one for an x-ray camera where the photoelectrons are of much higher energy.

The overall temporal resolution can be calculated by considering separately each portion of the camera system which can have an influence on the temporal resolution, calculating each section's contribution to the resolution, and then adding them in quadrature. Writing this as an equation:

$$\Delta t = (\Delta t_p^{\,2} + \Delta t_k^{\,2} + \Delta t_L^{\,2} + \Delta t_D^{\,2} + \Delta t_{DR}^{\,2} + \Delta t_{TR}^{\,2})^{\frac{1}{2}}$$

where the various subscripts stand for the following:

P = photocathode

k = vacuum interface at the photocathode (extraction region)

L = electron lens region

D = deflection region

DR = drift region

TR = technical resolution

The temporal resolution of a photocathode is just the RMS sum of the time it takes for the incident x-ray to be absorbed, the primary or Auger photoelectrons to be emitted, and the time it takes for the secondary electrons to be generated by multiple collisions inside the photocathode and leave the photocathode. The absorption and emission times are both on the order of 10^{-14} to 10^{-15} seconds. The longest transit time possible would be for a low energy electron, i.e. 10 ev, traversing the photocathode thickness, i.e. 1000Å, as a free electron with thermal velocity. This time would be only 5×10^{-14} seconds. This analysis, however, assumes a field free region inside the photocathode. As will be discussed later, these times might be altered if there is a field inside the photocathode.

The temporal dispersion in the extraction region is calculable from first principles. Since the emitted electrons have an energy spread, $\Delta\varepsilon$, this corresponds to a velocity spread of Δv where

$$\Delta v = \sqrt{\frac{2\Delta\varepsilon}{m}}$$

The time spread for these electrons to traverse a short space which has a constant electric field in it of magnitude E is

$$\Delta t_k = \frac{m\Delta V}{eE}$$

expressing this in cgse units

$$\Delta t_k = 1.12 \times 10^{-10} \frac{(\Delta\varepsilon)^{\frac{1}{2}}}{E} \text{ sec} \quad (\Delta\varepsilon \text{ in ev}) \quad (E \text{ in cgs})$$

or, expressing E in v/cm

$$\Delta t_k = 3.37 \times 10^{-8} \frac{(\Delta\epsilon)^{\frac{1}{2}}}{E} \text{ sec}$$

This is almost 50% greater than most authors quote. Most authors have quoted an analysis by Korobkin et. al. which made some assumptions about the distribution of emitted electrons which may not be true in the x-ray streak camera case. Inserting some typical numbers, i.e. a $\Delta\epsilon$ of 3.8 ev and an extraction field of 3333 v/cm this equation gives a Δt_k of 20 picoseconds.

The temporal dispersion in the lens region is much more difficult to estimate and really should be lumped together with the Δt_k contribution and calculated from the following integral. Let Δt be the time taken for a photoelectron of initial energy eV_o emitted normally from the photocathode to travel a distance x along the axis of the tube. Let $V(x)$ be the potential measured along the axis of the tube. Then:

$$\Delta t_L = (m/2e)^{\frac{1}{2}} \int_o^L (V_o + V(x))^{\frac{1}{2}} dx$$

The problem with this approach is that the potential $V(x)$ is not known. It could, however, be measured in an electrolytic tank or calculated from a model. Not knowing $V(x)$ or being able to measure it, other authors estimates for Δt_L will have to be employed. Kalibian et. al.[3] have estimated the dispersion for an electron lens of the Pierce type in an optical streak camera to be of the order of .1 picosecond. A more pessimistic view will be

taken here and a value of .5 picoseconds will be assumed for this tube. In a recent work by Jones, Sibbett and Bradley,[4] they have devised a computer code which calculates the time dispersion in a tube by computing the axial potential from a solution to Laplace's equation which matches the electron structures inside the tube. For a Photochron II tube with an optical photocathode they arive at a value of about .3 picoseconds for the time dispersion in the lens region. Kalibjian et. al.[3] have also calculated Δt_D the dispersion arising in the deflection region. They have calculated:

$$\Delta t_D = \frac{P\ V_D\ R_i}{v_o\ V_o\ d} \quad \text{sec}$$

where: P = deflection plate length (cm)

v_o = velocity of electrons (spread ignored) cm/sec

V_D = Deflector voltage (volts)

V_o = Beam potential (volts)

R_i = beam radius in deflector (cm)

d = deflection plate separation (cm)

For the ITL Photochron I

P = 18 mm

d = 4 mm

$V_o \doteq$ 18.5 Kv

V_D = 440 volts for a 1 cm deflection

$v_o = .8 \times 10^{10}$ cm/sec

R_i = 1 mm (assumed value - depends on current in beam)

These values give a value of 1.33 picoseconds for $\Delta\tau_D$. This seems to be a very large value, but note that this is for a rather large beam. Note also that the dispersion is a function of the total deflection so that the best time response is on the tube axis and that the time response is also a function of the beam radius which will be a function of the total beam current due to space charge beam spreading effects. Therefore, this contribution to the total dispersion could be a function of the total intensity. This is undoubtedly a very pessimistic estimate for the dispersion in the lens region because Jones et. al.[4] calculate the contribution from the deflection region to be of the order of .2 picoseconds.

Δt_{DR}, the dispersion due to the electrons traveling through the field free drift region between the anode and the screen can be calculated from:

$$\Delta t_{DR} = .84 \times 10^{-8} \frac{L\, V_a}{(V_s)^{3/2}} \text{ sec}$$

where L = drift length in cm

V_s = beam potential in the drift space in volts

eV_a = emission energy below which lie 90% of the secondary electrons in electron volts

Putting in typical values one finds $\Delta t_{DR} = .75$ picoseconds.

The last contribution to the overall time resolution is the so-called "technical resolution." The technical resolution is just the time it takes for the electron beam to be displaced one spatial resolution element at the phosphor screen while the tube

is being operated at a given sweep velocity. The Photochron I tube has a spatial resolution element size of about .1 mm square at the phosphor. Streak velocities of .2 mm/picosecond can be achieved with this tube giving a Δt_{TR} of .5 picoseconds.

Summarizing all these resolutions:

$$\Delta t_p = 5 \times 10^{-14} \text{ sec}$$
$$\Delta t_k = 2 \times 10^{-11} \text{ sec}$$
$$\Delta t_L = 3 \times 10^{-13} \text{ sec}$$
$$\Delta t_D = 1.3 \times 10^{-12} \text{ sec}$$
$$\Delta t_{DR} = 7.5 \times 10^{-13} \text{ sec}$$
$$\Delta t_{TR} = 5 \times 10^{-13} \text{ sec}$$

As can be seen from this table, only Δt_K has any real effect on the total temporal dispersion. Any real advances in increasing the time resolution of x-ray streak cameras will have to find ways of decreasing the dispersion in this region either by better photocathode designs and materials or by changes in the electron optics which allow a higher extraction field to be applied to the photocathode.

2. Spatial Resolution

The next most important characteristic in describing the overall performance of the x-ray streak camera system is the spatial resolution. Here, not only the spatial resolution of the image converter tube, image intensifier and film will be considered, but the resolution of the x-ray optics used to image the x-ray emissions from the target onto the photocathode will be considered.

The static spatial resolution of the Photochron I tube is generally quoted to be 8 line pairs per mm at the phosphor, and 30 line pairs per mm at the photocathode. These values are quoted at an extraction mesh to photocathode voltage such as to achieve a magnification of 3.75 in the image converter tube. However, these values are not obtainable in the dynamic, or streaking mode. Most measurements seem to indicate a reduction in spatial resolution by almost 50% to a value near 5 line pairs/mm. Various models have been proposed to account for this reduction and they all point to some space charge effects in or near the photocathode. Experiments have been carried out to substantiate these models, but so far all measurements have been done with visible photocathode tubes. The primary difference between the visible and x-ray photocathodes that might influence the dynamic spatial resolution is the resistivity of the photocathode. A 100 Å thick S-1 photocathode typical of a visible streak tube might have a surface resistivity of 150 ohm/square, while a 100 Å thick gold photocathode typical of an x-ray streak camera has a surface resistivity of only 2.2 ohm/square. No measurements have been published yet on the dynamic spatial resolution of an x-ray streak camera and this is one area of research which would bear investigation.

The spatial resolution of the image converter tube is certainly the limiting element in the electron optical chain of the camera system, but now the overall resolution of the system including the x-ray optics must be calculated.

The simplest imaging device to use in the x-ray regime is the x-ray pinhole camera. This is shown schematically in Figure 4. In the limit of geometric optics, two points separated by a distance, A_s, at the source (where the source is assumed to be small) are separated at the image plane, or photocathode in the case of an x-ray streak camera, by a distance given by:

$$\frac{A_s}{D_s} = \frac{A_p}{D_p}$$

$$\text{or} \quad A_p = A_s \, (D_p/D_s)$$

The quantity D_p/D_s is therefore the magnification M of the camera. Rays from a single source point passing through the pinhole of diameter $\emptyset$ subtend an angle $\emptyset/D_s$ and make an extended spot on the photocathode whose diameter is

$$B = \emptyset(D_s + D_p)/D_s$$

or

$$B = \emptyset(1 + M)$$

Alternatively, a point on the photocathode projects to the source with a diameter

$$B_s = \emptyset(1 + M)/M$$

If M is much larger than 1 then

$$B_s = \emptyset$$

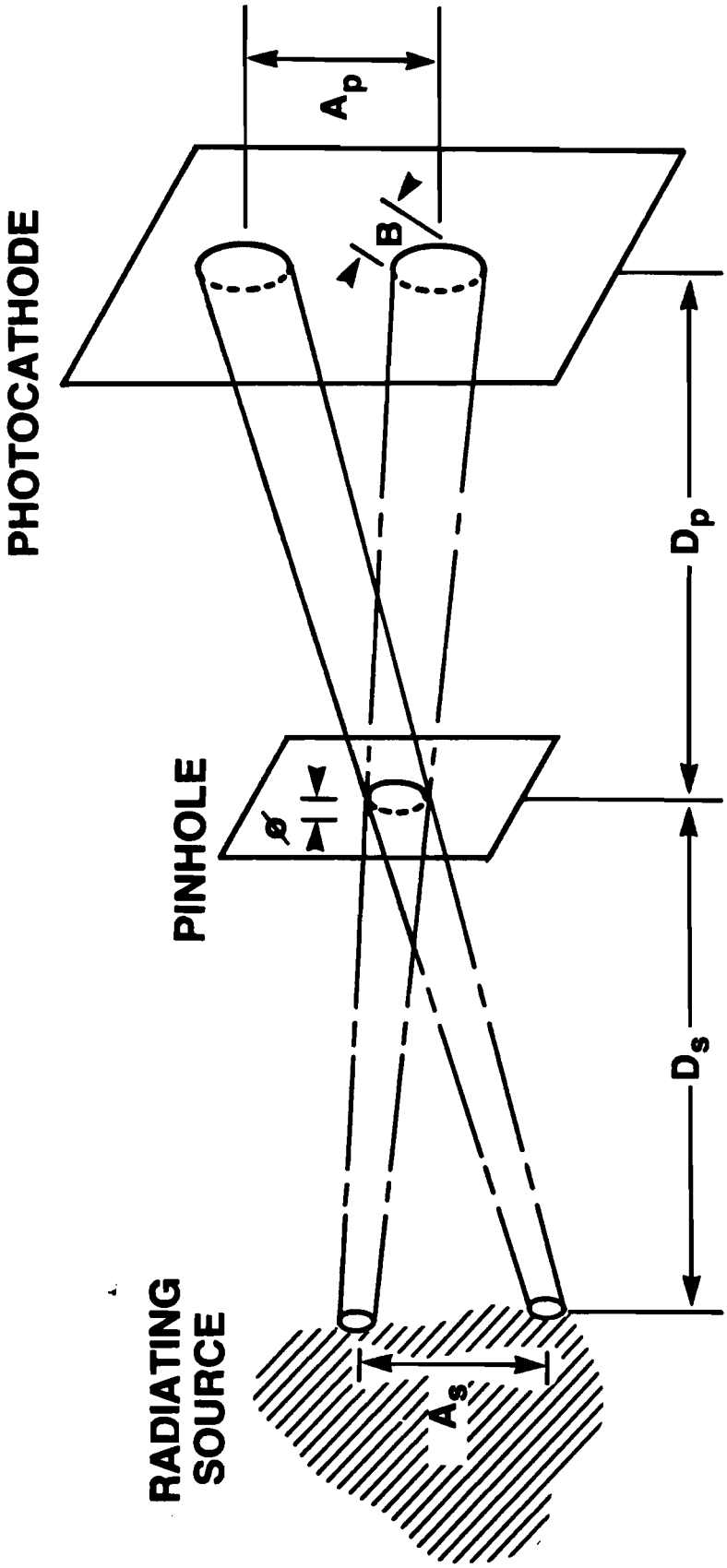

Figure 4. X-ray Pinhole Camera

and the resolution of the pinhole camera is said to equal to the equal to the diameter $\emptyset$ of the pinhole. Note that this definition of resolution is much more stringent than the definition usually applied to optical systems. In the x-ray pinhole camera case we have required that the images of two points be completely separated before it is claimed that two points are resolved. If the Rayleigh criterion of resolution were stringently applied to the pinhole camera the resolution would turn out to be less than the pinhole diameter. All of this analysis, however, has neglected diffraction effects which, although very small, can greatly diminish the resolving power of the pinhole camera. The half-angle of the central disc of the Fraunhoffer diffraction pattern is given by

$$\theta = 1.22\,\lambda/\emptyset$$

For the pinhole camera shown in Figure 4, the corresponding spot radius referred to the source is just

$$r_d = 1.22\,\lambda\,D_s/\emptyset$$

For typical x-ray streak camera applications $\lambda = 10$ Å, $D_s = 2$ cm and $\emptyset = 5$ microns yielding an r_d of 3.6 microns. The overall resolution can now be estimated by taking the RMS sum of the geometric and diffraction resolution to give

$$R = \sqrt{\emptyset^2 + (1.22\lambda\,D_s/\emptyset)^2}$$

This equation can be optimized for the value of $\emptyset$ which minimizes

R. This pinhole diameter turns out to be

$$\emptyset_{opt} = \sqrt{1.2\lambda D_s}$$

and the corresponding optimum resolution is

$$R_{opt} = 2.4\lambda D_s$$

However, in the experiments which were performed for this thesis research, a slit x-ray camera was used instead of a pinhole camera in order to obtain a larger collection angle and also for ease of alignment. A slit width of 25 microns was used with a magnification of 20x.

The general question of the deconvolution of an x-ray image through apertures of various shapes and sizes has recently been treated for the first time. Mueller[5,6] has published several studies concerning aperture imaging through apertures of various shapes including both wide and narrow slits. He finds that for a pinhole of the same diameter as the width of a slit the pinhole has much better resolution. In fact, a pinhole of radius R imaging a source of radius R_o, where $R/R_o = .3$ has better resolution than a slit of half-width W where $W/R_o = .1$. This fact was not appreciated until after the experimental work was completed, or else a narrower slit would have been attempted. In Mueller's terminology, a narrow slit is one whose half-width W satisfies $W/R_o < .1$, whereas a wide slit satisfies $W/R_o > (1 + M^{-1})^{-1}$. In the latter case, only the image edges contain spatial information (knife-edge imaging)

and derivatives must be taken to recover spatial information. Mueller points out that slits of intermediate width $.2 < W/R_o < (1 + M^{-1})^{-1}$ pose considerable problems in data reduction. In the case at hand where a 25μ wide slit imaged a 60μ diameter glass microballoon, $W/R_o = .25$ for the outer shell of the microballoon and $W/R_o = 1\text{-}2$ for the compressed inner core. Therefore, in neither case will image analysis be easy, particularly when noise is added. The core image will be slit width limited and the outer shell will be imaged with a resolution somewhat more than a slit-width.

3. Amplitude Resoultion

The last characteristic, and, unfortunately, the least understood, is the amplitude resolution or dynamic range. Much work has been done and reported concerning the dynamic range of optical streak cameras, but as yet no single model which will explain the measurements has been set forth. Also, as yet, no work has been published on the dynamic range of an x-ray streak camera. A simplified model for the dynamic range is the following.

The dynamic range of the camera is calculated as the ratio between the maximum flux incident on the photocathode which does not degrade either the temporal or spatial resolution and the minimum flux which is detectable at a given signal to noise ratio. An estimate of the maximum signal which does not degrade the camera performance can be calculated if the quantum efficiency and spatial resolution of the camera are known or can be calculated. This rather simplified model assumes that the limit on the maximum signal